

Goos-Hänchen like Shifts in Graphene Double Barriers

Ahmed Jellal^{*a,b,c}, Ilham Redouani^c, Youness Zahidi^c and Hocine Bahlouli^{a,d}

^a*Saudi Center for Theoretical Physics, Dhahran, Saudi Arabia*

^b*Physics Department, College of Science, King Faisal University,
PO Box 380, Alahsa 31982, Saudi Arabia*

^c*Theoretical Physics Group, Faculty of Sciences, Chouaib Doukkali University,
PO Box 20, 24000 El Jadida, Morocco*

^d*Physics Department, King Fahd University of Petroleum & Minerals,
Dhahran 31261, Saudi Arabia*

Abstract

We study the Goos-Hänchen like shifts for Dirac fermions in graphene scattered by double barrier structures. After obtaining the solution for the energy spectrum, we use the boundary conditions to explicitly determine the Goos-Hänchen like shifts and the associated transmission probability. We analyze these two quantities at resonances by studying their main characteristics as a function of the energy and electrostatic potential parameters. To check the validity of our computations we recover previous results obtained for a single barrier under appropriate limits.

PACS numbers: 72.80.Vp, 73.21.-b, 71.10.Pm, 03.65.Pm

Keywords: Graphene, double barriers, scattering, Goos-Hänchen like shifts, transmission.

*ajellal@ictp.it – a.jellal@ucd.ac.ma

1 Introduction

Graphene remains among the most fascinating and attractive subject in condensed matter physics [1]. This is because of its exotic physical properties and the apparent similarity of its mathematical model to the one describing relativistic fermions in two dimensions. As a consequence of this relativistic-like behavior, particle could tunnel through very high barriers in contrast to the conventional tunneling of non-relativistic particles, an effect known in relativistic field theory as Klein Tunneling. Such effect has already been observed experimentally [2] in graphene systems.

The Goos-Hänchen (GH) effect [3] is a phenomenon that originated in classical optics in which a light beam reflecting off a surface is spatially shifted as if it had briefly penetrated the surface before bouncing back. The interface has to separate different dielectric materials (such as glass or water), and absorption or transmission should be small enough to allow a substantial reflected beam to form [4]. The size of the GH effect is proportional to the derivative of the reflection phase with respect to the angle of incidence. In addition to shifting beam position, the GH effect can manifest itself in alterations of differential cross sections [5] of laser mode dynamics [6] and of mode spectra [7].

Various experimental and theoretical investigations classified the transport properties among the most interesting features of Dirac fermions in graphene. Among these transport properties we cite the quantum version of the GH effect originating from the reflection of particles from interfaces. The latter has been studied at a single graphene interface [8,9] and in graphene-based electric and magnetic potential barriers [10]. Subsequently, it was shown that the modulation of Goos-Hänchen like (GHL) shifts can be controlled by varying the electrostatic potential and induced gap [11] and can even be enhanced by transmission resonances. Very recently, the giant GHL shifts for electron beams tunneling through graphene double barrier structures [12] was also investigated and it was found that the shifts exhibits a sharp peaks inside the transmission gap.

There are various ways for creating barrier structures in graphene [13,14], for instance it can be done by applying a gate voltage, cutting the graphene sheet into finite width to create a nanoribbons, using doping or through the creation of a magnetic barrier. Different experimental methods are available to open a gap in graphene systems. One of them is through an inversion symmetry breaking of the sublattice due to the fact that the densities of the particles associated with the on-site energy for A and B sublattice are different [15]. As demonstrated in the experiment, the maximum energy gap could be 260meV due to the sublattice symmetry breaking [15]. Therefore, the periodic dependence of GHL shifts on the induced gap also provides an efficient way to modulate the lateral shifts in a fixed gapped graphene barrier, which is useful for the manipulation of electron beam propagation in graphene [16].

Based on previous investigations of Dirac fermions and in particular our recent work [17–19], where we developed our approach to deal with graphene double barrier structures, in the present work we analyze the GHL shifts by considering Dirac fermions in the presence of an electrostatic potential placed between two regions composing the graphene sheet. For general purposes, we consider the potential configuration depicted in Figure 1 rather than that used in [12]. By requiring the continuity of the wave functions at interfaces, we show that it is possible to determine the GHL shifts as well as the transmission probability in terms of the incident angle. By focussing on resonances, we conclude that these two quantities become large and their shapes exhibit different peaks. We emphasis the difference

between our results and those obtained in [12] by studying double barriers. Considering an appropriate limiting case, we derive interesting results regarding single barriers. Comments and discussions will be provided in the main text to support the relevance of our present potential configuration.

The paper is organized as follows. In section 2, we formulate our model by setting the Hamiltonian system describing particles scattered by double barrier structures. Considering the five potential regions one at a time, we obtain the spinor solution corresponding to each region in terms of different scattering potential parameters. Using boundary conditions we are required to split the energy into three domains in order to calculate the transmission probability in section 3 and GH shift in section 4 in each domain. In each situation, we analyze the GH shifts and transmission at resonances that characterize each region. In section 5, we discuss the importance of our numerical results and present different supporting plots. We also study some limiting cases, particular interest is the situation where our problem reduces to the single barrier problem. Finally, we conclude our work in section 6 and emphasize our main results.

2 Theoretical model

We consider Dirac fermions in graphene scattered by an electrostatic double barrier potential. We can write the Hamiltonian describing our particle in the central region 3 as follows

$$H_3 = v_F \vec{\sigma} \cdot \vec{p} + V_3(x) \mathbb{I}_2 + \Delta \sigma_z \quad (1)$$

where $v_F \approx 10^6 m/s$ is the Fermi velocity, $\sigma = (\sigma_x, \sigma_y)$ are the Pauli matrices and $\vec{p} = -i\hbar \vec{\nabla}$. The parameter $\Delta = mv_F^2$ is the energy gap owing to the sublattice symmetry breaking or it can be seen as the energy gap $\Delta = \Delta_{so}$ originating from spin-orbit interaction. Elsewhere the system is described by the Hamiltonian

$$H_j = v_F \vec{\sigma} \cdot \vec{p} + V_j(x) \mathbb{I}_2. \quad (2)$$

In order to study the scattering of Dirac fermions in graphene by the above double barrier structure we first choose the following potential configuration for the double barrier potential

$$V_j(x) = \begin{cases} v & \text{if } d_1 < |x| < d_2 \\ u & \text{if } |x| < d_1 \\ 0 & \text{otherwise} \end{cases} \quad (3)$$

where j labels the five regions indicated schematically in Figure 1, which shows the space configuration of the potential profile

Solving the eigenvalue equation to obtain the upper and lower components of the eigenspinor in the incident and reflection regions 1 ($x < -d_2$)

$$\Phi_1 = \begin{pmatrix} 1 \\ z_1 \end{pmatrix} e^{i(k_1 x + k_y y)} + r \begin{pmatrix} 1 \\ -z_1^{-1} \end{pmatrix} e^{i(-k_1 x + k_y y)}. \quad (4)$$

In region 2 ($-d_2 < x < -d_1$), we obtain the solution

$$\Phi_2 = a \begin{pmatrix} 1 \\ z_2 \end{pmatrix} e^{i(k_2 x + k_y y)} + b \begin{pmatrix} 1 \\ -z_2^{-1} \end{pmatrix} e^{i(-k_2 x + k_y y)}. \quad (5)$$

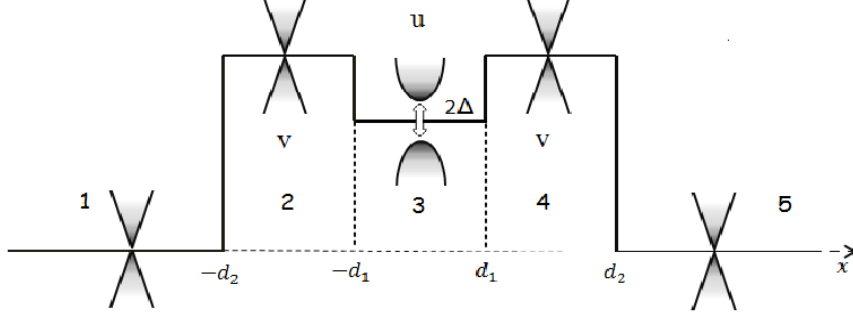


Figure 1: Schematic diagram for the monolayer graphene double barrier.

In region 4 ($d_1 < x < d_2$), we have the eigenspinor

$$\Phi_4 = e \begin{pmatrix} 1 \\ z_2 \end{pmatrix} e^{i(k_2x+k_2y)} + f \begin{pmatrix} 1 \\ -z_2^{-1} \end{pmatrix} e^{i(-k_2x+k_2y)} \quad (6)$$

and finally the eigenspinor in region 5 ($x > d_2$) can be expressed as

$$\Phi_5 = t \begin{pmatrix} 1 \\ z_1 \end{pmatrix} e^{i(k_1x+k_1y)}. \quad (7)$$

We have introduced the perpendicular $k_j = k_{F_j} \cos \theta_j$ and parallel $k_y = k_{F_j} \sin \theta_j$ components of the wave vector as well as the parameter

$$z_j = s_j \frac{k_j + ik_y}{\sqrt{k_j^2 + k_y^2}} = s_j e^{i\theta_j} \quad (8)$$

where the sign function is defined by $s_j = \text{sign}(E - V_j)$ with the phase $\theta_j = \arctan(k_y/k_j)$ and $k_{F_j} = \frac{2\pi}{\lambda_j}$ is the Fermi wave vector. The corresponding dispersion relation in these four regions is given by

$$E - V_j = s_j \sqrt{k_j^2 + k_y^2} = s_j \hbar v_F k_{F_j}. \quad (9)$$

Now solving the eigenvalue equation for the Hamiltonian (1) describing region 3, we find the following eigenspinor

$$\Phi_3 = c_1 \begin{pmatrix} \alpha \\ \beta z_3 \end{pmatrix} e^{i(k_3x+k_3y)} + c_2 \begin{pmatrix} \alpha \\ -\beta z_3^{-1} \end{pmatrix} e^{i(-k_3x+k_3y)} \quad (10)$$

with the parameters α and β are given by

$$\alpha = \left(1 + \frac{s_3 \Delta}{\sqrt{\Delta^2 + \hbar^2 v_F^2 k_{F_3}^2}} \right)^{1/2}, \quad \beta = \left(1 - \frac{s_3 \Delta}{\sqrt{\Delta^2 + \hbar^2 v_F^2 k_{F_3}^2}} \right)^{1/2} \quad (11)$$

the complex number is defined by

$$z_3 = s_3 e^{i\theta_3}, \quad \theta_3 = \arctan(k_y/k_3) \quad (12)$$

with the sign function $s_3 = \text{sign}(E - u)$. The Fermi wave vector being defined by

$$k_{F_3} = \frac{1}{\hbar v_F} \sqrt{(E - u)^2 - \Delta^2} \quad (13)$$

and k_3 is given by the relation

$$k_3 = \sqrt{k_{F_3}^2 - k_y^2}. \quad (14)$$

As usual the coefficients (c_1, c_2) together with (a, b, e, f, r, t) can be determined using the boundary conditions, continuity of the eigenspinors at each interface. Next we will use the above solutions to compute the transmission coefficient and associated phase shift and build a bridge between quantum optics and Dirac fermions in graphene.

3 Transmission amplitude and phase shift

Before determining explicitly the transmission coefficient and the phase shift, let us discuss the main features of the solutions obtained above. We characterize our waves by introducing a critical angle ϕ_c , defined by

$$\phi_c = \arcsin \sqrt{\frac{k_{F_2}}{k_{F_1}}} = \arcsin \frac{\sqrt{(E - v)^2}}{E} \quad (15)$$

which corresponds to total internal reflection. We notice that when the incident angle is less than ϕ_c , i.e $\theta_1 < \phi_c$, the modes become oscillating guided modes. While in the case when the incident angle is more than ϕ_c , i.e $\theta_1 > \phi_c$, we have decaying or evanescent wave modes, this amounts to replace k_3 by $i\kappa$ with

$$\kappa = \sqrt{k_y^2 - k_{F_3}^2}. \quad (16)$$

In the forthcoming analysis, we will be interested in studying the situation $\theta_1 < \phi_c$ and investigate the GHM shifts for particles scattered by the potential profile (3). This will necessitate the evaluation of the transmission coefficient and the phase shift. Matching the wave functions at the boundaries $(-d, -d/2, d/2, d)$ as required by the first order nature of the Dirac equation we end up with the following set of equations

$$e^{-ik_1 d} + r e^{ik_1 d} = a e^{-ik_2 d} + b e^{ik_2 d} \quad (17)$$

$$a e^{-ik_2 d/2} + b e^{ik_2 d/2} = c_1 \alpha e^{-ik_3 d/2} + c_2 \beta e^{ik_3 d/2} \quad (18)$$

$$c_1 \alpha e^{ik_3 d/2} + c_2 \beta e^{-ik_3 d/2} = e e^{ik_2 d/2} + f e^{-ik_2 d/2} \quad (19)$$

$$e e^{ik_2 d} + f e^{-ik_2 d} = t e^{ik_1 d}. \quad (20)$$

After a lengthy but straightforward algebra, we can show that the transmission coefficient can be written in terms of the phase shift φ as indicated below

$$t = \frac{e^{i\varphi}}{f_0} \quad (21)$$

and we have

$$\begin{aligned} f_0 e^{i\varphi} = & \chi_1 \cos[(k_2 - k_3)d] + (1 - \chi_1) \cos[(k_2 + k_3)d] \\ & + i \{(-\chi_1 \sin[(k_2 - k_3)d] + (\chi_1 - 1) \sin[(k_2 + k_3)d]) \chi_2 - \chi_3 \chi_4 \sin(k_3 d)\} \end{aligned} \quad (22)$$

where the χ 's are given by

$$\begin{aligned}
\chi_1 &= \frac{1}{2} \left(1 + \tan \theta_2 \tan \theta_3 - \frac{s_2 s_3}{\alpha \beta} \sec \theta_2 \sec \theta_3 \right) \\
\chi_2 &= \tan \theta_1 \tan \theta_2 - s_1 s_2 \sec \theta_1 \sec \theta_2 \\
\chi_3 &= s_1 \sec \theta_1 \tan \theta_2 - s_2 \sec \theta_2 \tan \theta_1 \\
\chi_4 &= -s_2 \sec \theta_2 \tan \theta_3 + \frac{s_3}{\alpha \beta} \sec \theta_3 \tan \theta_2.
\end{aligned} \tag{23}$$

Using (22) and (23), we can show that the phase shift can be expressed explicitly as follows

$$\varphi = \arctan \left(-\frac{(\chi_1 \sin [(k_2 - k_3)d] + (1 - \chi_1) \sin [(k_2 + k_3)d]) \chi_2 + \chi_3 \chi_4 \sin (k_3 d)}{\chi_1 \cos [(k_2 - k_3)d] + (1 - \chi_1) \cos [(k_2 + k_3)d]} \right). \tag{24}$$

We will see how this phase will be used to investigate the GHl shifts for Dirac fermions scattered by double barriers as depicted in Figure 1. The computation of the GHl shift will be performed in the next section where we will also emphasize the main difference between our results and those obtained by Song [12].

4 GHl shifts through double barriers

We begin our study of the GHl shift by considering an incident, reflected and transmitted beams around some transverse wave vector $k_y = k_{y_0}$ corresponding to the central incidence angle θ_{1_0} , denoted by the subscript 0. These can be expressed in integral forms as follows

$$\Psi_i(x, y) = \int_{-\infty}^{+\infty} dk_y g(k_y - k_{y_0}) e^{i(k_1(k_y)x + k_y y)} \begin{pmatrix} 1 \\ z_1 \end{pmatrix} \tag{25}$$

$$\Psi_r(x, y) = \int_{-\infty}^{+\infty} dk_y r(k_y) g(k_y - k_{y_0}) e^{i(-k_1(k_y)x + k_y y)} \begin{pmatrix} 1 \\ -z_1^{-1} \end{pmatrix} \tag{26}$$

$$\Psi_t(x, y) = \int_{-\infty}^{+\infty} dk_y t(k_y) g(k_y - k_{y_0}) e^{i(k_1(k_y)x + k_y y)} \begin{pmatrix} 1 \\ z_1 \end{pmatrix} \tag{27}$$

where each spinor plane wave is a solution of (2) and $g(k_y - k_{y_0})$ is the angular spectral distribution, which can be assumed of Gaussian shape $w_y e^{-w_y^2(k_y - k_{y_0})^2}$ with w_y being the half beam width at waist [8]. The reflection $r(k_y)$ and transmission $t(k_y)$ coefficients will be calculated through the use of boundary conditions.

In order to calculate the GHl shifts of the transmitted beam through the graphene double barriers, we adopt the definition [20, 21]

$$s_t = -\frac{\partial \varphi}{\partial k_{y_0}}. \tag{28}$$

We emphasize that our calculation will be done for different values of the signature s_j in the three regions of interest but at first we consider a zero gap, i.e. $\Delta = 0$. Clearly, the value of s_j can be obtained from the relation

$$s_j = \frac{E - V_j}{\sqrt{k_{j_0}^2 + k_{y_0}^2}} \tag{29}$$

which tells us that $s_j = 1$ on the particle-like branch, $E > V_j$, whereas $s_j = -1$ on the hole-like branch, $E < V_j$. Therefore, to discuss the relevance of our results, we consider different cases as summarized below in Table 1

Region 1	Region 2	Region 3	$E(u < v)$	$E(u > v)$
$s_1 = 1$	$s_2 = -1$	$s_3 = -1$	$E < u < v$	$E < v < u$
		$s_3 = 1$	$u < E < v$	
	$s_2 = 1$	$s_3 = -1$		$v < E < u$
		$s_3 = 1$	$u < v < E$	$v < u < E$

Table 1: Different signature cases s_j and their associated energy intervals.

Now according to the above table, one has to consider three different cases in order to determine the GHL shifts in our system. These cases are characterized by their energy regions as follows: $E < u < v$, $u < E < v$ and finally $u < v < E$. Note that, we are focussing here only on $u < v$ while the case $u > v$ will be considered later in section 6.

► For case 1: $E < u < v$, we use (28) to obtain the following GHL shifts

$$s_t = -\frac{d^2}{f_0^2} \tan \theta_{1_0} (-A_1 B_1 + C_1 D_1) \quad (30)$$

where different quantities are defined by

$$\begin{aligned} A_1 &= \frac{1+\mu_-^2}{k_{2_0} d} \cos(k_{3_0} d) \sin(k_{2_0} d) + \frac{1+\nu_-^2}{k_{3_0} d} \cos(k_{2_0} d) \sin(k_{3_0} d) + \frac{2-\mu_-^2-\nu_-^2}{k_{2_0} k_{3_0} d^2} \sin(k_{2_0} d) \sin(k_{3_0} d) \\ B_1 &= \frac{k_{1_2}^+ k_{2_3}^- k_{y_0}^2}{k_{2_0}^2 k_{3_0}} \sin(k_{3_0} d) + \frac{k_{0_+}^2}{k_{2_0}} \left(\cos(k_{3_0} d) \sin(k_{2_0} d) + \frac{k_{3_0} \mu_-^2}{k_{2_0}} \sin(k_{3_0} d) \cos(k_{2_0} d) \right) \\ C_1 &= \cos(k_{2_0} d) \cos(k_{3_0} d) - \frac{k_{3_0} \mu_-^2}{k_{2_0}} \sin(k_{2_0} d) \sin(k_{3_0} d) \\ D_1 &= \frac{k_{0_+}^2}{k_{2_0}} \left(-\frac{1+\mu_-^2}{k_{2_0} d} \cos(k_{2_0} d) \cos(k_{3_0} d) + \frac{1+\nu_-^2}{k_{3_0} d} \sin(k_{2_0} d) \sin(k_{3_0} d) - \frac{2-\mu_-^2-\nu_-^2}{k_{2_0} k_{3_0} d^2} \cos(k_{2_0} d) \sin(k_{3_0} d) \right) \\ &\quad + \frac{k_{1_2}^+ k_{2_3}^-}{k_{2_0}^2 k_{3_0} d^2} \left(2 \sin k_{3_0} d + k_{y_0}^2 \left(\frac{1}{k_{1_0}^2} + \frac{2}{k_{2_0}^2} + \frac{1}{k_{3_0}^2} \right) \sin(k_{3_0} d) - \frac{k_{y_0}^2 d}{k_{3_0}} \cos(k_{3_0} d) \right) \\ &\quad + \frac{1}{k_{2_0} d^2} \left(2 + \frac{k_{0_+}^2}{k_{2_0}^2} + \frac{k_{0_+}^2}{k_{1_0}^2} \right) \left(\cos(k_{3_0} d) \sin(k_{2_0} d) + \frac{k_{3_0} \mu_-^2}{k_{2_0}} \cos(k_{2_0} d) \sin(k_{2_0} d) \right) \end{aligned}$$

and we have set

$$\mu_{\pm} = \sqrt{k_{F_2} k_{F_3} \pm k_{y_0}^2 / k_{3_0}}, \quad \nu_{\pm} = \sqrt{k_{F_2} k_{F_3} \pm k_{y_0}^2 / k_{2_0}} \quad (31)$$

$$k_{1_2}^{\pm} = k_{F_1} \pm k_{F_2}, k_{2_3}^{\pm} = k_{F_2} \pm k_{F_3}, \quad k_{0_{\pm}} = \sqrt{k_{F_1} k_{F_2} \pm k_{y_0}^2}. \quad (32)$$

The corresponding transmission probability reads

$$\begin{aligned} T &= \left[\left(\cos(k_{2_0} d) \cos(k_{3_0} d) - \frac{k_{3_0} \mu_-^2}{k_{2_0}} \sin(k_{2_0} d) \sin(k_{3_0} d) \right)^2 \right. \\ &\quad \left. + \left(\frac{k_{1_2}^+ k_{2_3}^- k_{y_0}^2}{k_{1_0} k_{2_0}^2 k_{3_0}} \sin(k_{3_0} d) + \frac{k_{0_+}^2}{k_{1_0} k_{2_0}} \left(\sin(k_{2_0} d) \cos(k_{3_0} d) + \frac{k_{3_0} \mu_-^2}{k_{2_0}} \sin(k_{3_0} d) \cos(k_{2_0} d) \right) \right)^2 \right]^{-1}. \end{aligned} \quad (33)$$

It is clearly seen that to obtain full transmission one should impose resonance conditions, which are given by

$$k_{2_0}d = N_1\pi, \quad k_{3_0}d = N_2\pi \quad (34)$$

with $N_1, N_2 = 0, \pm 1, \pm 2, \dots$. Under these circumstances, (30) can be reduced to the simple form

$$s_t|_{k_{2_0}d=N_1\pi, k_{3_0}d=N_2\pi} = d \tan \theta_{1_0} \left[\frac{k_{0_+}^2}{k_{2_0}^2} (1 + \mu_-^2) + (-1)^{N_1} \frac{k_{1_2}^+ k_{2_3}^- k_{y_0}^2}{k_{2_0}^2 k_{3_0}^2} \right] \quad (35)$$

which corresponds to the maximum absolute value of the GHL shift.

► Now we consider the case 2: $u < E < v$, which gives

$$s_t = -\frac{d^2}{f_0^2} \tan \theta_{1_0} (-A_2 B_2 + C_2 D_2) \quad (36)$$

with

$$\begin{aligned} A_2 &= \frac{1-\mu_+^2}{k_{2_0}d} \cos(k_{3_0}d) \sin(k_{2_0}d) + \frac{1-\nu_+^2}{k_{3_0}d} \cos(k_{2_0}d) \sin(k_{3_0}d) + \frac{2+\mu_+^2+\nu_+^2}{k_{2_0}k_{3_0}d^2} \sin(k_{2_0}d) \sin(k_{3_0}d) \\ B_2 &= \frac{k_{1_2}^+ k_{2_3}^+ k_{y_0}^2}{k_{2_0}^2 k_{3_0}^2} \sin(k_{3_0}d) + \frac{k_{0_+}^2}{k_{2_0}} \left(\cos(k_{3_0}d) \sin(k_{2_0}d) - \frac{k_{3_0} \mu_+^2}{k_{2_0}} \sin(k_{3_0}d) \cos(k_{2_0}d) \right) \\ C_2 &= \cos(k_{2_0}d) \cos(k_{3_0}d) + \frac{k_{3_0} \mu_+^2}{k_{2_0}} \sin(k_{2_0}d) \sin(k_{3_0}d) \\ D_2 &= \frac{k_{0_+}^2}{k_{2_0}} \left(-\frac{1-\mu_+^2}{k_{2_0}d} \cos(k_{2_0}d) \cos(k_{3_0}d) + \frac{1-\nu_+^2}{k_{3_0}d} \sin(k_{2_0}d) \sin(k_{3_0}d) - \frac{2+\mu_+^2+\nu_+^2}{k_{2_0}k_{3_0}d^2} \cos(k_{2_0}d) \sin(k_{3_0}d) \right) \\ &\quad + \frac{k_{1_2}^+ k_{2_3}^+}{k_{2_0}^2 k_{3_0}^2 d^2} \left(2 \sin k_{3_0}d + k_{y_0}^2 \left(\frac{1}{k_{1_0}^2} + \frac{2}{k_{2_0}^2} + \frac{1}{k_{3_0}^2} \right) \sin(k_{3_0}d) - \frac{k_{y_0}^2 d}{k_{3_0}} \cos(k_{3_0}d) \right) \\ &\quad + \frac{1}{k_{2_0}d^2} \left(2 + \frac{k_{0_+}^2}{k_{2_0}^2} + \frac{k_{0_+}^2}{k_{1_0}^2} \right) \left(\cos(k_{3_0}d) \sin(k_{2_0}d) - \frac{k_{3_0} \mu_+^2}{k_{2_0}} \cos(k_{2_0}d) \sin(k_{3_0}d) \right) \end{aligned}$$

while the transmission probability is given by

$$\begin{aligned} T &= \left[\left(\cos(k_{2_0}d) \cos(k_{3_0}d) + \frac{k_{3_0} \mu_+^2}{k_{2_0}} \sin(k_{2_0}d) \sin(k_{3_0}d) \right)^2 + \left(\frac{k_{1_2}^+ k_{2_3}^+ k_{y_0}^2}{k_{1_0} k_{2_0}^2 k_{3_0}^2} \sin(k_{3_0}d) \right. \right. \\ &\quad \left. \left. + \frac{k_{0_+}^2}{k_{1_0} k_{2_0}} \left(\sin(k_{2_0}d) \cos(k_{3_0}d) - \frac{k_{3_0} \mu_+^2}{k_{2_0}} \sin(k_{3_0}d) \cos(k_{2_0}d) \right) \right)^2 \right]^{-1} \quad (37) \end{aligned}$$

The GHL shifts at resonances are given by

$$s_t|_{k_{2_0}d=N_1\pi, k_{3_0}d=N_2\pi} = d \tan \theta_{1_0} \left(\frac{k_{0_+}^2}{k_{2_0}^2} (1 - \mu_+^2) + (-1)^{N_1} \frac{k_{1_2}^+ k_{2_3}^+ k_{y_0}^2}{k_{2_0}^2 k_{3_0}^2} \right). \quad (38)$$

► For the case 3: $u < v < E$, the corresponding GHL shifts are found to be

$$s_t = -\frac{d^2}{f_0^2} \tan \theta_{1_0} (-A_3 B_3 + C_3 D_3) \quad (39)$$

where various parameters are defined by

$$\begin{aligned} A_3 &= \frac{1+\mu_-^2}{k_{2_0}d} \cos(k_{3_0}d) \sin(k_{2_0}d) + \frac{1+\nu_-^2}{k_{3_0}d} \cos(k_{2_0}d) \sin(k_{3_0}d) + \frac{2-\mu_-^2-\nu_-^2}{k_{2_0}k_{3_0}d^2} \sin(k_{2_0}d) \sin(k_{3_0}d) \\ B_3 &= -\frac{k_{1_2}^- k_{2_3}^- k_{y_0}^2}{k_{2_0}^2 k_{3_0}^2} \sin(k_{3_0}d) - \frac{k_{0_-}^2}{k_{2_0}} \left(\cos(k_{3_0}d) \sin(k_{2_0}d) + \frac{k_{3_0} \mu_-^2}{k_{2_0}} \sin(k_{3_0}d) \cos(k_{2_0}d) \right) \\ C_3 &= \cos(k_{2_0}d) \cos(k_{3_0}d) - \frac{k_{3_0} \mu_-^2}{k_{2_0}} \sin(k_{2_0}d) \sin(k_{3_0}d) \\ D_3 &= \frac{k_{0_-}^2}{k_{2_0}} \left(\frac{1+\mu_-^2}{k_{2_0}d} \cos(k_{2_0}d) \cos(k_{3_0}d) - \frac{1+\nu_-^2}{k_{3_0}d} \sin(k_{2_0}d) \sin(k_{3_0}d) + \frac{2-\mu_-^2-\nu_-^2}{k_{2_0}k_{3_0}d^2} \cos(k_{2_0}d) \sin(k_{3_0}d) \right) \\ &\quad - \frac{k_{1_2}^- k_{2_3}^-}{k_{2_0}^2 k_{3_0}^2 d^2} \left(2 \sin(k_{3_0}d) + k_{y_0}^2 \left(\frac{1}{k_{1_0}^2} + \frac{2}{k_{2_0}^2} + \frac{1}{k_{3_0}^2} \right) \sin(k_{3_0}d) - \frac{k_{y_0}^2 d}{k_{3_0}} \cos(k_{3_0}d) \right) \\ &\quad + \frac{1}{k_{2_0}d^2} \left(2 - \frac{k_{0_-}^2}{k_{2_0}^2} - \frac{k_{0_-}^2}{k_{1_0}^2} \right) \left(\cos(k_{3_0}d) \sin(k_{2_0}d) + \frac{k_{3_0} \mu_-^2}{k_{2_0}} \cos(k_{2_0}d) \sin(k_{3_0}d) \right). \end{aligned}$$

The transmission probability reduces to

$$T = \left[\left(\cos(k_{2_0}d) \cos(k_{3_0}d) - \frac{k_{3_0}\mu_-^2}{k_{2_0}} \sin(k_{2_0}d) \sin(k_{3_0}d) \right)^2 + \left(-\frac{k_{1_2}^- k_{2_3}^- k_{y_0}^2}{k_{1_0} k_{2_0}^2 k_{3_0}} \sin(k_{3_0}d) + \frac{k_{0_-}^2}{k_{1_0} k_{2_0}} \left(-\sin(k_{2_0}d) \cos(k_{3_0}d) + \frac{k_{3_0}\mu_-^2}{k_{2_0}} \sin(k_{3_0}d) \cos(k_{2_0}d) \right) \right)^2 \right]^{-1}. \quad (40)$$

At resonances, the GHL shifts can be written as follows

$$st|_{k_{2_0}d=N_1\pi, k_{3_0}d=N_2\pi} = -d \tan \theta_{1_0} \left[\frac{k_{0_-}^2}{k_{2_0}^2} (1 + \mu_-^2) + (-1)^{N_1} \frac{k_{1_2}^- k_{2_3}^- k_{y_0}^2}{k_{2_0}^2 k_{3_0}^2} \right]. \quad (41)$$

Having obtained the closed form expressions of the GHL shifts in different energy domains, we proceed now to compute these quantities numerically. This will help us understand the effect of various potential parameters on the GHL shifts in our double barrier structure.

5 Discussions

To allow for a suitable interpretation of our main results, we compute numerically the GHL shifts under various conditions. First we plot the GHL shifts as a function of the energy for specific values of the potential parameters ($d = 10nm$, $v = 8meV$, $u = 4meV$) and three different values of the incidence angle $\theta_{1_0} = 4^\circ, 6^\circ, 8^\circ$, see Figure 2. It is clear from this figure that the GHL shifts change sign at the Dirac points, namely ($E = u, E = v$). We deduce that there is a strong dependence of the GHL shifts on the incidence angle θ_{1_0} , it increases with θ_{1_0} . As observed in the work of Chen [22], it is shown that the GHL shifts are related to the transmission gap $\Delta E = 2\hbar k_y v_F$. We notice that the GHL shifts displays sharp peaks inside the transmission gap around the point $E = v$, while they are absent around the energy point $E = u$. In such situation, one can clearly end up with an interesting result such that the number of sharp peaks is equal of that of transmission resonances. We also observe that the shifts become constant after certain threshold energy value, which is compatible with a maximum of transmission.

It is interesting to investigate how the GH shifts behave as a function of the barrier potential heights, i.e. v and u , the numerical results are shown in Figure 3. We have chosen the parameters ($E = 4, v = 8$) in Figure 3(a) and ($E = 8, u = 4$) in Figure 3(b), with inter-barrier distance $d = 10nm$ and angles $\theta_{1_0} = 4^\circ, 6^\circ, 8^\circ$. One can notice that, at the Dirac points ($E = u, E = v$), the GH shifts change their sign and behave differently as compared to Figure 2. This change in sign of the GH shifts shows clearly that they are strongly dependent on the barrier heights. We also notice that the GH shifts are positive as long as the energy satisfies the condition $E > v > u$ and negative for $E < u < v$. However, in the energy domain $u < E < v$ Figures 3(a) and 3(b) show different behaviors such that the shifts are negative and positive, respectively. Note that, the Dirac points represent the zero modes for Dirac operator [10] and lead to the emergence of new Dirac points, this point has been discussed in different works [24–26]. Such point separates the two regions of positive and negative refraction. In the cases of $v < E$ and $v > E$ (respectively $u < E$ and $u > E$), the shifts are respectively in the forward and backward directions, due to the fact that the signs of group velocity are opposite.

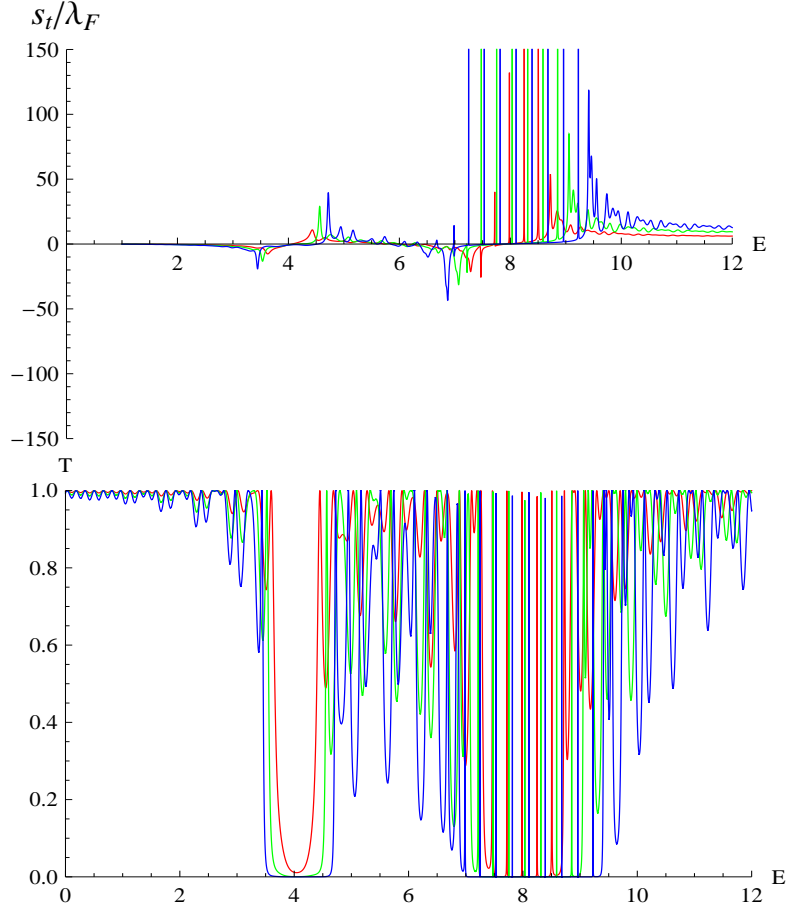


Figure 2: The GHL shifts and the transmission as a function of energy, with $d = 10nm$, $v = 8meV$, $u = 4meV$, $\theta_{10} = 4^\circ$ (red line), $\theta_{10} = 6^\circ$ (green line), $\theta_{10} = 8^\circ$ (blue line).

Now let us investigate what will happen if we introduce a gap in the band structure. Note that, the gap is introduced as shown in Figure 1 and therefore it affects the system energy according to the solution of the energy spectrum obtained in region 3. Figure 4 shows that the GHL shifts in the propagating case can be enhanced by a gap opening at the Dirac point. This has been performed by fixing the parameters $d = 10nm$, $v = 8meV$, $u = 4meV$ and making different choices for the energy and angle. For the configuration ($E = 3meV$, $\theta_{10} = 6^\circ$) we conclude that we can still have negative shifts as it is shown by the orange line. However for other configurations, we do not have such behavior, more specifically by increasing Δ , the GHL shifts become mostly constant up to some value then show sharp peaks as indicated in blue color where we have taken $E = 10meV$ and $\theta_{10} = 6^\circ$.

To make comparison with the relevant literature and show the importance of our results, we will discuss three interesting special cases. Since our work is a generalization of [11] to double barriers, we first show how to recover their results. This can be done by requiring that $u = v$, which implies that $k_{F_2} = k_{F_3}$ or $k_{2_0} = k_{3_0}$ and therefore the present system behaves like a single barrier where the GHL shift reduces to

$$s_t = 2dT \tan \theta_{10} \left[\left(2 \pm \left(\frac{k_{0\pm}^2}{k_{1_0}^2} + \frac{k_{0\pm}^2}{k_{2_0}^2} \right) \right) \frac{\sin(4k_{2_0}d)}{4k_{2_0}d} \mp \frac{k_{0\pm}^2}{k_{2_0}^2} \right] \quad (42)$$

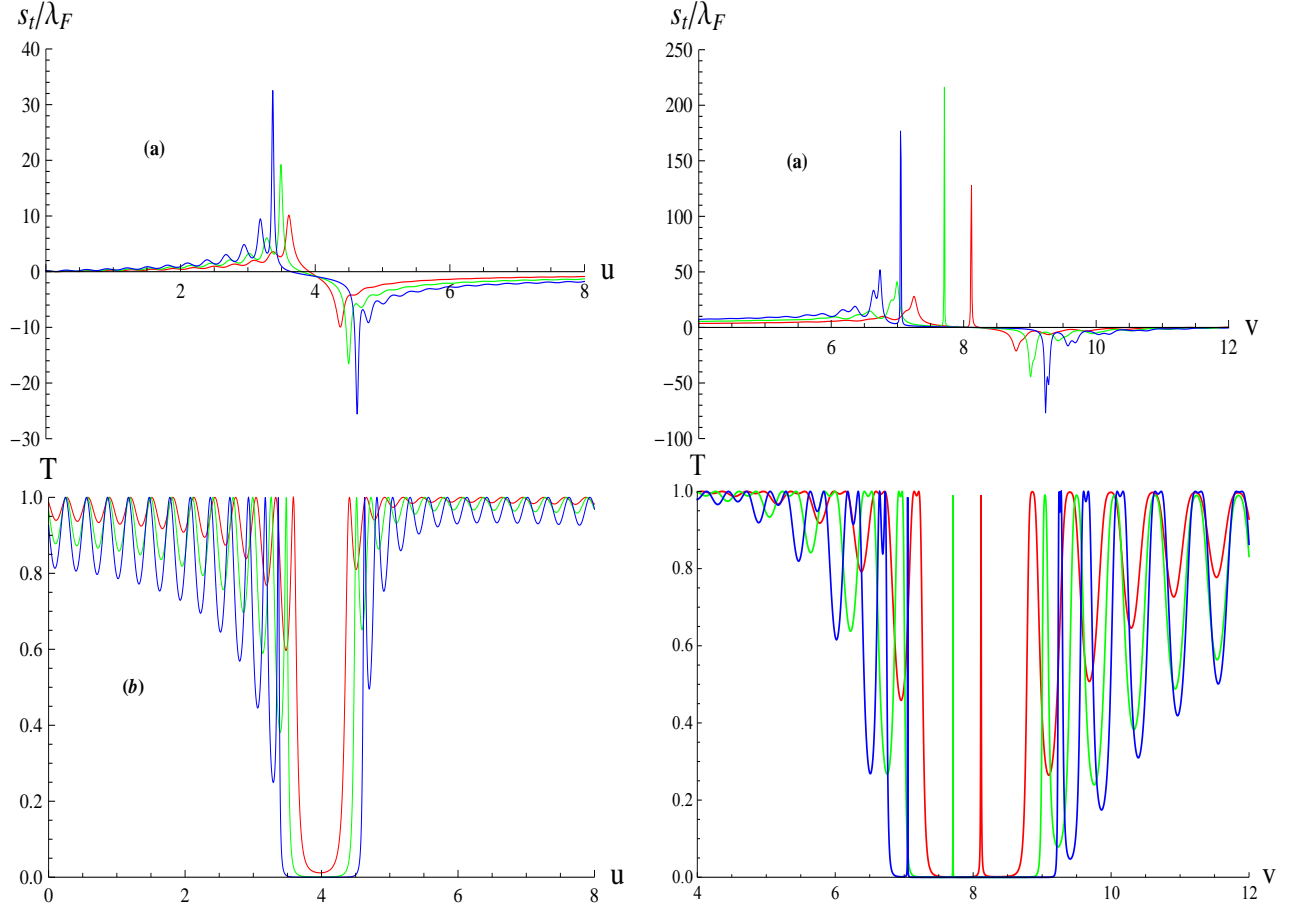


Figure 3: The GHL shifts and the transmission as a function of the heights u and v of the potential barrier. (a)/(b) for height u/v , with $(E = 4, v = 8)/(E = 8, u = 4)$, where $d = 10 \text{ nm}$, $\theta_{1_0} = 4^\circ$ (red line), $\theta_{1_0} = 6^\circ$ (green line), $\theta_{1_0} = 8^\circ$ (blue line).

and the corresponding transmission coefficient is given by

$$T = \left[\cos^2(2k_{2_0}d) + \frac{k_{0\pm}^4}{k_{2_0}^2 k_{1_0}^2} \sin^2(2k_{2_0}d) \right]^{-1} \quad (43)$$

where \pm correspond to Klein tunneling and classical behavior, respectively. Note that these results are identical to those obtained previously in [11]. The above GHL shifts and transmission are plotted in Figure 5. It is clearly seen that s_t is oscillating between negative and positive values around the critical point $E = u = v$. At such a point T is showing zero transmission while it oscillates away from the critical point.

In the second particular case we consider $u = 0$, which implies equality between wave vectors $k_{F_1} = k_{F_3}$, and is equivalent to the requirement that $k_{1_0} = k_{3_0}$. This is similar to one potential configuration for the system studied in [12] to deal with the GHL shifts. In the present case, s_t becomes

$$s_t = -d^2 T \tan \theta_{1_0} \left(-A'_{\pm} B'_{\pm} + C'_{\pm} D'_{\pm} \right) \quad (44)$$

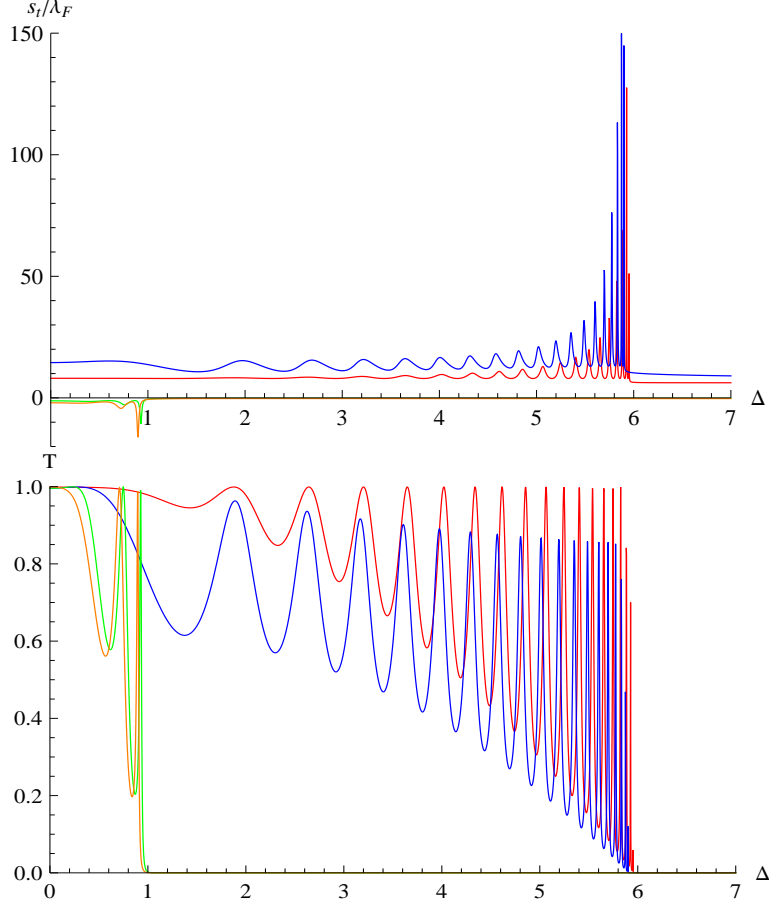


Figure 4: The influence of the induced gap Δ on the GHl shifts and the transmission in the presence of a double barrier, for $d = 10\text{nm}$, $v = 8\text{meV}$, $u = 4\text{meV}$, $E = 10\text{meV}$, $\theta_{1_0} = 4^\circ$ (red line), $E = 10\text{meV}$, $\theta_{1_0} = 6^\circ$ (blue line), $E = 3\text{meV}$, $\theta_{1_0} = 4^\circ$ (green line), $E = 3\text{meV}$, $\theta_{1_0} = 6^\circ$ (orange line).

where we have set

$$\begin{aligned}
A'_\pm &= \frac{1 \mp \mu_\pm^2}{k_{2_0} d} \cos(k_{3_0} d) \sin(k_{2_0} d) + \frac{1 \mp \nu_\pm^2}{k_{3_0} d} \cos(k_{2_0} d) \sin(k_{3_0} d) + \frac{2 \pm \mu_\pm^2 \pm \nu_\pm^2}{k_{2_0} k_{3_0} d^2} \sin(k_{2_0} d) \sin(k_{3_0} d) \\
B'_\pm &= \frac{k_{2_3}^2 k_{y_0}^2}{k_{2_0}^2 k_{3_0}} \sin(k_{3_0} d) \pm k_{2_0} \nu_\pm^2 \left(\cos(k_{3_0} d) \sin(k_{2_0} d) \mp \frac{k_{3_0} \mu_\pm^2}{k_{2_0}} \sin(k_{3_0} d) \cos(k_{2_0} d) \right) \\
C'_\pm &= \cos(k_{2_0} d) \cos(k_{3_0} d) \pm \frac{k_{3_0} \mu_\pm^2}{k_{2_0}} \sin(k_{2_0} d) \sin(k_{3_0} d) \\
D'_\pm &= \mp k_{2_0} \nu_\pm^2 \left(\frac{1 \mp \mu_\pm^2}{k_{2_0} d} \cos(k_{2_0} d) \cos(k_{3_0} d) - \frac{1 \mp \nu_\pm^2}{k_{3_0} d} \sin(k_{2_0} d) \sin(k_{3_0} d) + \frac{2 \pm \mu_\pm^2 \pm \nu_\pm^2}{k_{2_0} k_{3_0} d^2} \cos(k_{2_0} d) \sin(k_{3_0} d) \right) \\
&\quad + \frac{k_{2_3}^2}{k_{2_0}^2 k_{3_0} d^2} \left(2 \sin k_{3_0} d + 2k_{y_0}^2 \left(\frac{1}{k_{2_0}^2} + \frac{1}{k_{3_0}^2} \right) \sin(k_{3_0} d) - \frac{k_{y_0}^2 d}{k_{3_0}} \cos(k_{3_0} d) \right) \\
&\quad + \frac{1}{k_{2_0} d^2} (2 \pm \mu_\pm^2 \pm \nu_\pm^2) \left(\cos(k_{3_0} d) \sin(k_{2_0} d) \mp \frac{k_{3_0} \mu_\pm^2}{k_{2_0}} \cos(k_{2_0} d) \sin(k_{3_0} d) \right).
\end{aligned}$$

Transmission probability is given by

$$\begin{aligned}
T &= \left[\left(\cos(k_{2_0} d) \cos(k_{3_0} d) \pm \frac{k_{3_0} \mu_\pm^2}{k_{2_0}} \sin(k_{2_0} d) \sin(k_{3_0} d) \right)^2 + \left(\frac{k_{2_3}^2 k_{y_0}^2}{k_{2_0}^2 k_{3_0}} \sin(k_{3_0} d) \right. \right. \\
&\quad \left. \left. \pm \mu_\pm \nu_\pm \left(\sin(k_{2_0} d) \cos(k_{3_0} d) - \frac{k_{3_0} \mu_\pm^2}{k_{2_0}} \sin(k_{3_0} d) \cos(k_{2_0} d) \right) \right)^2 \right]^{-1}
\end{aligned} \tag{45}$$

where the sign \pm corresponds to the two energy intervals, $0 < E < v$ ($-$) and $E > v$ ($+$), respectively. The GHl shifts and transmission as functions of the energy E are shown in Figure 6 for the values

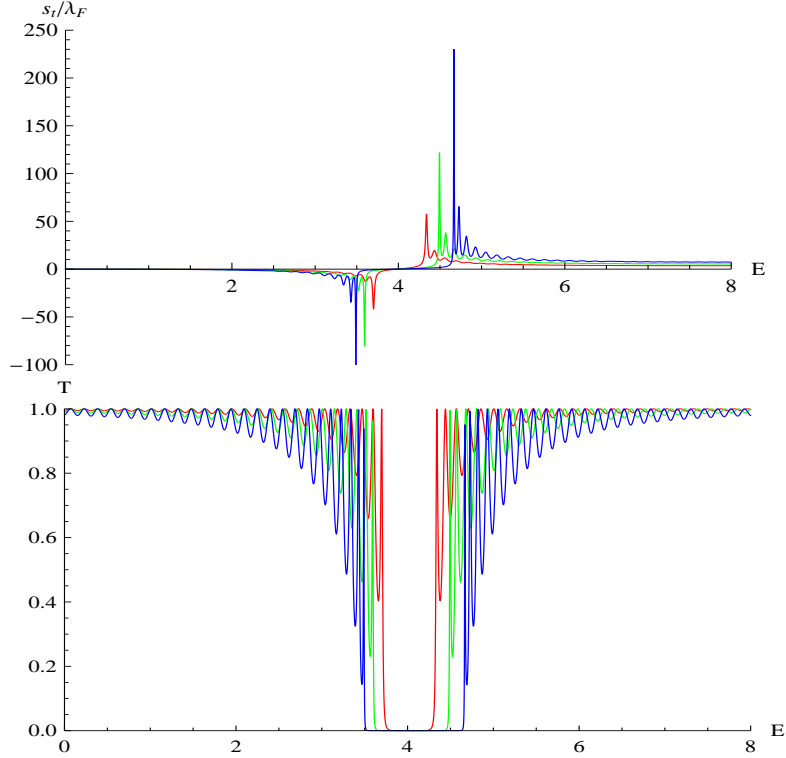


Figure 5: The GHL shifts and the transmission as function of the energy E , for $d = 10nm$, $v = u = 4meV$, $\theta_{1_0} = 4^\circ$ (red line), $\theta_{1_0} = 6^\circ$ (green line), $\theta_{1_0} = 8^\circ$ (blue line).

$d = 10nm$, $v = 8meV$, $u = 0meV$ and $\theta_{1_0} = 4^\circ, 6^\circ, 8^\circ$. Both quantities are showing a series of peaks and resonances. The resonances correspond to the bound states of the double barriers. We notice that the GHL shifts peak at each bound state energy and are clearly shown in the transmission curve underneath. The energies at which transmission vanishes correspond to energies at which the GHL shifts change sign. Since these resonances are very sharp (true bound states with zero width) it is numerically very difficult to track all of them, if we do then the alternation in sign of the GHL shifts will be observed. As before, we notice that around the Dirac point $E = v$ the number of peaks is equal of that of transmission resonances. To summarize, we notice that a superposition of the two Figures 5 and 6, obtained in both particular cases for $u = v$ and $u = 0$, respectively, gives exactly Figure 2.

Finally we consider the third case where $u > v$. In such situation the GHL shifts and transmission are displayed in Figure 7. It is clearly seen that the GHL shifts display sharp peaks inside the transmission gap around the point the Dirac point $E = v$ but no peaks inside the transmission gap around the point Dirac point $E = u$. This happened in the negative region rather than positive one as seen in Figure 2, which is due to the exchange of role between barrier heights u and v , i.e. $u > v$. Due to this exchange the structure of the transmission is reversed between Figure 2 and Figure 7, sharp resonances appear in the higher transmission gap in Figure 2 while they appear in the lower transmission gap in Figure 7. As observed in previous figures, we have the same numbers of sharp peaks in s_t and transmission resonances. Thus in our situation we have transmission gaps and zero-k gaps which are identified with Dirac points, in our case with energies $E = v$ and $E = u$. We have

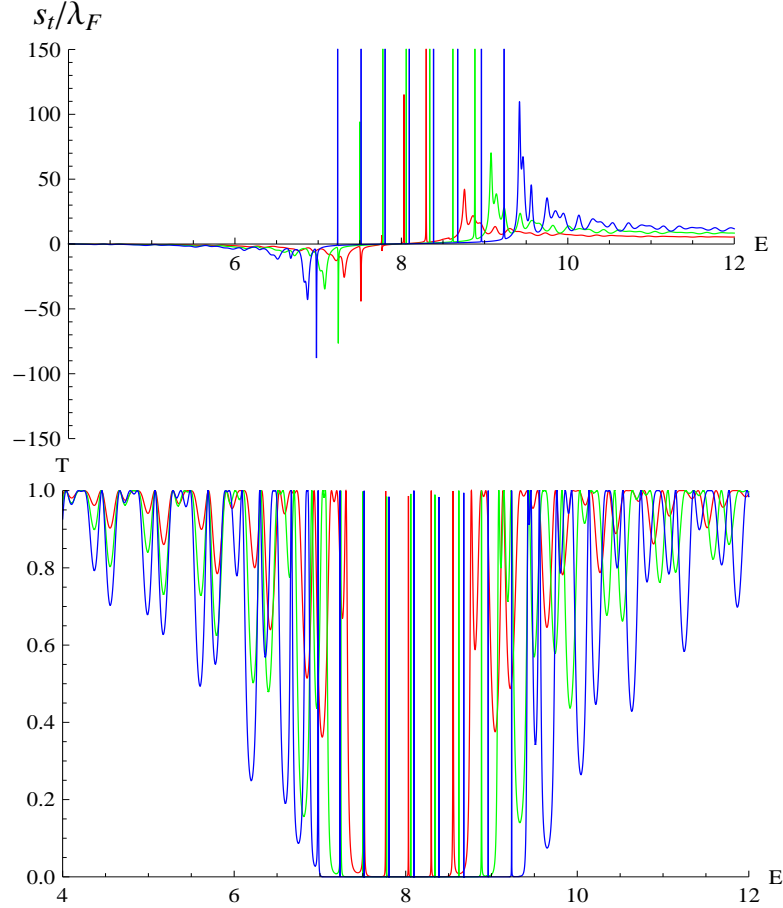


Figure 6: The GHL shifts and the transmission as function of the energy E , with $d = 10nm$, $v = 8meV$, $u = 0meV$, $\theta_{10} = 4^\circ$ (red line), $\theta_{10} = 6^\circ$ (green line), $\theta_{10} = 8^\circ$ (blue line).

observed that GHL shifts change sign when crossing the edges of the transmission gap but is not affected by the zero- k gaps. This observation was not affected by the incident angle as long as it is below the critical angle defining total reflection. It is worth mentioning that these observations regarding zero- k gap are in contrast to those in superlattices where GHL shifts change sign at the edge of the zero- k band gap.

In summary, we note that the GHL shifts display sharp peaks inside the transmission gap around the point Dirac $E = v$ in our system as shown in Figure 1. These peaks can be attributed to the quasibound states formed in the double barrier structure. To confirm these findings we have also studied the simple barrier structure as a special case of our potential configuration by setting $u = v$, these peaks are then absent. The GHL shifts inside the transmission gap around the point $E = u$ in our system is the same as in the simple barrier case [11].

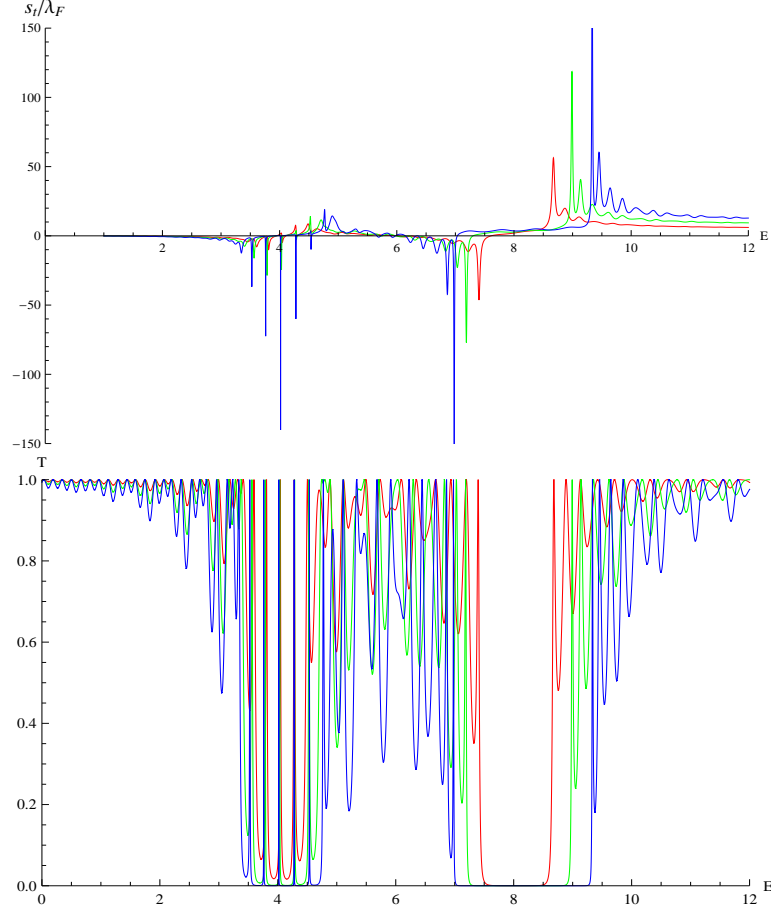


Figure 7: The GHL shifts and the transmission as a function of the energy E in the case where $u > v$, with $d = 10nm$, $v = 4meV$, $u = 8meV$, $\theta_{10} = 4^\circ$ (red line), $\theta_{10} = 6^\circ$ (green line), $\theta_{10} = 8^\circ$ (blue line).

6 Conclusion

We have computed the Goos-Hänchen like (GHL) shifts through a double barrier potential in a single layer graphene system. The massless Dirac-like equation was used to describe the scattered fermions by such potential configuration. Our results show that the GHL shifts is affected by the internal structure of the double barrier, in particular the GHL shifts change sign at the transmission zero energies and peaks at each bound state associated with the double barrier. Thus our numerical results show that the GHL shifts can be enhanced by the presence of resonant energies in the system when the incident angle is less than the critical angle associated with total reflection.

It was also observed that the transmission gap increases with the incidence angle as long as it less than the critical angle. The gap within the well region is seen to reduce both transmission and GHL shifts which exhibit an oscillatory behavior as a function of the energy gap. The GHL shifts also depend on the potential parameters, more specifically the heights of the barrier and well regions, u and v . In particular for $v > u$ we observe that there is no Klein region while for $u > v$ we do have a Klein tunneling region which enhances transmission and GHL shifts. Thus with double barrier structure we can have more control on the GHL shifts. To support the validity of our findings we have selected our potential parameters so as to reduce it to a single barrier and confirmed all results found

previously by other groups [11]. In the case of a single barrier peaks corresponding to bound states are absent in the zero transmission region. Also we have checked the results obtained in [12] for the particular case $u = 0$.

Finally, we close our work by mentioning some challenges facing the potential connection between two fields: quantum optics and graphene. Very recently, pertinent discussions have been made to emphasize the main difficulties in detecting the Goos-Hanchen shifts and preparing the electron beam in solid-state physics [27]. These discussions open for us important research avenues that will help us understand and overcome the above mentioned difficulties. On the other hand, we learned from [27] that the spin-orbit coupling in optics is an interesting and fascinating topic because the spin-orbit interaction in graphene opens up a spin-orbit gap, though very small, at the Dirac points. All these matters will be highly important when we consider tunable GH shift leading to potential applications in future graphene based electronic devices. These matters will be investigated in the near future to enable us to get a deeper understanding of graphene transport properties.

Acknowledgments

The authors would like to acknowledge the support of King Fahd University of Petroleum and minerals under the theoretical physics research group project RG1306-1 and RG1306-2. The generous support provided by the Saudi Center for Theoretical Physics (SCTP) is highly appreciated by all authors. AJ thanks the Deanship of Scientific Research at King Faisal University for funding this research number (140232).

References

- [1] K. S. Novoselov, A. K. Geim, S. V. Morozov, D. Jiang, Y. Zhang, S. V. Dubonos, I. V. Grigorieva and A. A. Firsov, *Science* 306, 666 (2004).
- [2] N. Stander, B. Huard and D. Goldhaber-Gordon, *Phys. Rev. Lett.* 102, 026807 (2009).
- [3] F. Goos and H. Hänchen, *Ann. Phys.* 436, 333 (1947).
- [4] D. H. Foster, J. U. Nöckel and A. K. Cook, *Opt. Lett.* 32, 1764 (2007).
- [5] N. H. Tran, L. Dutriaux, P. Balcou, A. Le Floch and F. Bretenaker, *Opt. Lett.* 20, 1233 (1995).
- [6] L. Dutriaux, A. Le Floch and F. Bretenaker, *J. Opt. Soc. Am. B* 12, 2283 (1992).
- [7] D. Q. Chowdhury, D. H. Leach and R. K. Chang, *J. Opt. Soc. Am. A* 11, 1110 (1994).
- [8] C. W. J. Beenakker, R. A. Sepkhanov, A. R. Akhmerov and J. Tworzydło, *Phys. Rev. Lett.* 102, 146804 (2009).
- [9] L. Zhao and S. F. Yelin, *Phys. Rev. B* 81, 115441 (2010).
- [10] M. Sharma and S. Ghosh, *J. Phys.: Condens Matter* 23, 055501 (2011).
- [11] X. Chen, J.-W. Tao and Y. Ban, *Eur. Phys. J. B* 79, 203 (2011).

- [12] Y. Song, H. C. Wu and Y. Guo, *Appl. Phys. Lett.* 100, 253116 (2012).
- [13] M. I. Katsnelson, K. S. Novoselov and A. K. Geim, *Nature Phys.* 2, 620 (2006).
- [14] H. Sevincli, M. Topsakal and S. Ciraci, *Phys. Rev. B* 78, 245402 (2008).
- [15] S. Y. Zhou, G.-H. Gweon, A. V. Fedorov, P. N. First, W. A. de Heer, D.-H. Lee, F. Guinea, A. H. Castro Neto and A. Lanzara, *Nat. Mater.* 6, 770 (2007).
- [16] Z.-F. Wang and F. Liu, *ACS Nano* 4, 2459 (2010).
- [17] A. D. Alhaidari, H. Bahlouli and A. Jellal, *Advances in Mathematical Physics*, 762908 (2012).
- [18] A. Jellal, E. B. Choubabi, H. Bahlouli and A. Aljaafari, *J. Low Temp. Phys.* 168, 40 (2012).
- [19] H. Bahlouli, E. B. Choubabi, A. Jellal and M. Mekkaoui, *J. Low Temp. Phys.* 169, 51 (2012).
- [20] X. Chen, Y. Ban and C.-F. Li, *J. Appl. Phys.* 105, 093710 (2009).
- [21] X. Chen, C.-F. Li and Y. Ban, *Phys. Rev. B* 77, 073307 (2008).
- [22] X. Chen, L.-G. Wang and C.-F. Li, *Phys. Rev. A* 80, 043839 (2009).
- [23] M. R. Setare and D. Jahani, *J. Phys.: Condens. Matter* 22, 245503 (2010).
- [24] S. Bhattacharjee, M. Maiti and K. Sengupta, *Phys. Rev. B* 76, 184514 (2007).
- [25] C. H. Park, L. Yang, Y. W. Son, M. L. Cohen and S. G. Louie, *Phys. Rev. Lett.* 101, 126804 (2008).
- [26] C. H. Park, Y. W. Son, L. Yang, M. L. Cohen and S. G. Louie, *Phys. Rev. Lett.* 103, 046808 (2009).
- [27] X. Chen, X.-J. Lu, Y. Ban and C.-F. Li, *J. Opt.* 15, 033001 (2013).